J. Micromech. Microeng. **20** (2010) 095028 (12pp) doi:10.1088/0960-1317/20/9/095028

Low-cost carbon thick-film strain sensors for implantable applications

Christian A Gutierrez and Ellis Meng

Department of Biomedical Engineering, University of Southern California, 1042 Downey Way, DRB-140, Los Angeles, CA 90089-1111, USA

E-mail: ellis.meng@usc.edu

Received 17 March 2010, in final form 23 July 2010
Published 27 August 2010
Online at stacks.iop.org/JMM/20/095028

Abstract

The suitability of low-cost carbon thick-film strain sensors embedded within a biomedical grade silicone rubber (Silastic® MDX4-4210) for implantable applications is investigated. These sensors address the need for robust cost-effective implantable strain sensing technology for the closed loop operation of function-restoring neural prosthetic systems. Design, fabrication and characterization of the sensors are discussed in the context of the application to strain/fullness measurements of the urinary bladder as part of the neuroprosthetic treatment of lower urinary tract dysfunction. The fabrication process, utilizing off-the-shelf screen-printing materials, is convenient and cost effective while achieving resolutions down to 75 μm. This method can also be extended to produce multilayer embedded devices by superposition of different screen-printable materials. Uniaxial loading performance, temperature dependence and long-term soak testing are used to validate suitability for implantation while proof-of-concept operation (up to 40% strain) is demonstrated on a bench-top latex balloon bladder model.

(Some figures in this article are in colour only in the electronic version)

1. Introduction

In 2008, it was estimated that approximately 259 000 Americans suffer from chronic spinal cord injury (SCI), and each year this number increases by about 12 000 [1]. SCI patients with lower urinary tract dysfunction face many challenging medical problems that have both an adverse and a profound impact on daily life [2]. In normal patients, stretch-sensitive mechanoreceptors located in the bladder wall respond to filling and transmit the sense of fullness to the autonomic spinal cord centers. In SCI patients, however, the sensory input to drive micturition (bladder voiding) is lost due to damage to the signal conducting spinal cord.

Restoration of bladder function through the use of neuroprosthetic systems has been an active area of research for some time. However, a significant and unmet requirement for these systems is the need for feedback information regarding the fullness/state of the bladder. Closed-loop, tether-free operation necessitates the integration of a sensor system that provides this information to the function-restoring neuroprosthetic system capable of triggering bladder voiding in response to the detection of maximal bladder filling (figure 1). It is known that the internal bladder pressure undergoes only small changes during filling (∼400 Pa) due to creep and stress relaxation in the bladder wall; much larger changes are encountered during voiding (∼5000 Pa) [3]. Furthermore, pressure measurements can be confounded by body-movement-induced artifacts [4]. Thus, interestingly, pressure data alone do not provide an adequate or reliable measure of fullness. In fact, bladder wall strain correlates more effectively with bladder volume and is a direct and easily observable measure of bladder fullness [5].

Despite the biomechanical evidence, the majority of efforts to determine bladder fullness use pressure as the primary indicator [6–8]. This may be due, in part, to the ability to readily catheterize pressure sensors for internal measurements, but these approaches require repeat procedures, are generally uncomfortable and can be painful for patients. Clearly, there exists a need for the development of more aptly suited technologies to address the unique challenges presented by physiological mechanical systems. A simple yet robust approach is adopted here to the measurement of strain for *in vivo* applications. The focus of this paper is the design, fabrication and application of carbon thick-film strain

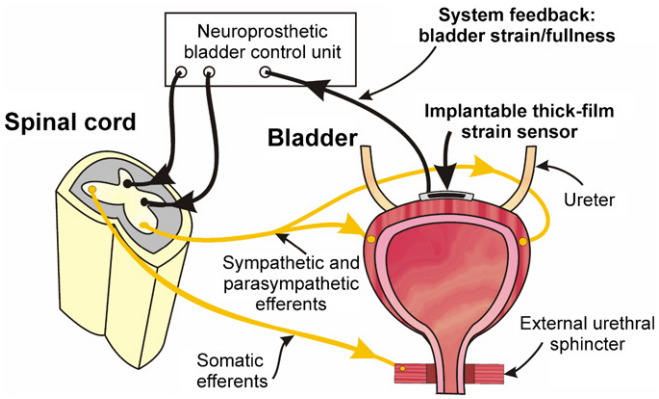

Figure 1. Urinary bladder anatomy showing the muscles and efferents involved in micturition. A separate function-restoring neuroprosthetic system uses existing efferent circuitry via spinal cord stimulation to control bladder voiding. The system utilizes strain sensor feedback for the purpose of detecting bladder fullness via bladder wall strain measurements to activate bladder voiding as required.

sensors for implantable sensor systems in the context of the neuroprosthetic treatment of urinary tract dysfunction due to SCI. Due to the ease of use and ability to create precise patterns on a variety of substrates, thick-film-based technologies are regarded as being compact, robust and relatively inexpensive [9]. These features make thick-film-based sensor technologies an attractive option for implantable sensor systems.

2. Materials, design and fabrication

2.1. Material selection

Class III medical devices designed to be implanted into the body must satisfy strict FDA regulations for biocompatibility and bio-inertness. Therefore, material selection and the use of proven biomedical grade materials is an important design consideration at the outset of any implantable device design. For these reasons, biomedical grade silicone rubber (MDX4–4210, Silastic®, Dow Corning, Midland, MI) was selected as the strain sensor substrate due to its proven *in vivo* performance and compliance with United States Pharmacopeia (USP) class VI and ISO 10993-1 material standards. Complete encapsulation of thick-film devices within this substrate maximizes material safety and eliminates the potential for an immune response to the embedded thick-film material.

For the application discussed here, high-resistance carbon thick-film paste (7082, DuPont, Wilmington, DE) was selected as a suitable thick-film material because of its high resistance, suitability for screen-printing [10] and strain-responsive characteristics. Carbon-based pastes were previously used as force sensitive resistors (FSRs) in artificial hair cell devices [11] and in tactile sensors, and they are known to exhibit robust piezoresistive properties [12, 13]. The high-resistance nature of carbon thick films readily enables resistance measurements directly with a multimeter without the need for bridge or signal amplification circuitry, thereby further simplifying the sensor interface.

A commonly cited figure-of-merit for the strain sensitivity of strain sensors is known as the gauge factor (GF) and is dependent on the choice of piezoresistive material. It is defined as

$$\mathrm{GF} = \frac{\Delta R/R}{\Delta L/L} = \frac{\Delta R/R}{\varepsilon},$$

where R is the nominal undeformed strain gauge resistance, ΔR is the total change in resistance, L is the original unstrained length of the strain gauge, ΔL is the total change in length under strain and ε is the applied strain across the gauge area. Thick-film materials have been shown to exhibit GFs in the range of 2–10 [14–16], which is nominally better than traditional thin-film metal strain gauges (GF $\sim$ 2). However, the benefits of high-strain operation (>0.1%), compatibility with implantable substrates (such as silicone rubbers), and cost-effective fabrication and packaging techniques make thick films considerably more attractive for the application discussed here.

2.2. Fabrication of the screen-printing apparatus

Thick films can easily be patterned by screen printing. This method of pattern transfer involves the use of a physical mask acting as a stencil or screen through which the thick-film paste is applied. The predefined open areas in the screen thus transfer a thick-film image onto the underlying substrate. Despite the numerous technical advances and high costs associated with production-grade screen-printing equipment, the ultimate printing resolution of these systems still lies around 50 μm. The approach adopted here utilizes low-cost, off-the-shelf screen-printing materials employing a lithographically defined brass screen and an acrylic frame, with reproducible printing resolution down to $\sim$75 μm.

A brass shim stock sheet assortment was purchased from Precision Brand (Downers Grove, IL) along with a metal etching kit from MicroMark (Berkeley Heights, NJ) containing all necessary lithographic and etching tools and materials. Brass sheets of 25–75 μm thickness were used. Brass sheets were cut to size (11.5 $\times$ 15.2 mm) and cleaned using a wet abrasive pad to remove the native oxide layer. A negative dry-film photoresist was then cut to size and applied to both sides of the wet metal sheet. The photoresist-metal sandwich was then placed in between two protective laminator sheets and passed through a standard business card laminator provided as part of the kit. The resist was then patterned lithographically under ultraviolet light (45 mJ cm^{-2}), utilizing a standard transparency mask (Mikacolor, Los Angeles, CA). Photoresist development was then performed in a dilute sodium hydroxide solution, and the brass sheet was placed in a ferric chloride bath at $\sim$80 °C under constant agitation to etch away areas of exposed metal. After etching, a metal polish was applied to the clean metal surface to protect the metal screen from corrosion and oxidation. A laser-machined acrylic frame was constructed to hold and stretch the metal screen above the substrate (figure 2).

A precision metal-blade handheld squeegee (Permalex®, Transition Automation, Tyngsboro, MA) was used to press the carbon paste through the lithographically defined patterns

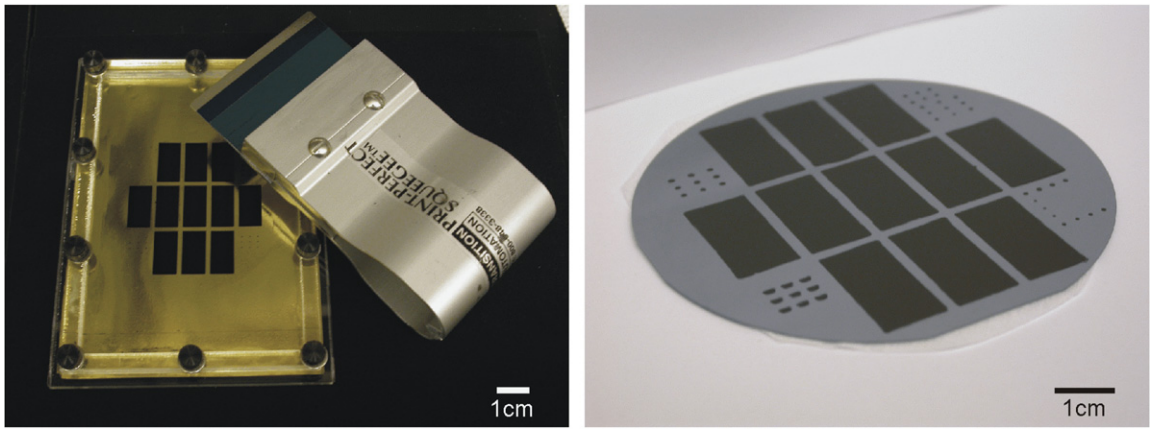

(*a*) (*b*)

Figure 2. (*a*) Custom made screen printing apparatus with brass screen, acrylic frame and metal blade squeegee. (*b*) Screen-printed carbon coupons on a silicon wafer.

in the metal screen onto the underlying substrate. The pre-cured as-printed carbon film thickness was dictated by the thickness of the screen used. The final post-curing carbon film thickness was typically 50–60% of the pre-cured thickness due to shrinkage and evaporation of solvents during the curing process.

2.3. Alternative deposition and patterning methods

2.3.1. Spinning. Spin coating was investigated as an alternative method to producing uniform thick films (figure 3). This was attempted on both silicon and glass substrates at various speeds. Due to the highly viscous nature of the standard paste, a thinner (3610—Dipropylene glycol monomethyl ether, TCI, Portland, OR) was used to lower the paste viscosity. It was found that although films were successfully spun onto the substrate, their uniformity was poor when compared to uniformities achieved with standard photoresists. Significant thickness variation and striation were clearly visible, especially at speeds below 2 krpm, and these were likely due to the lack of any leveling agents or striation-reducing additives that are commonly employed in standard photoresist formulations. Additionally, the grain size of the carbon particles (graphite) was of the order of 1–2 μm, so any aggregation or clumping of these grains also contributed to the observed striation and surface roughness.

2.3.2. Plasma etching. Because of the organic nature of the carbon paste, it was hypothesized that reactive ion etching (RIE) in oxygen plasma could provide a means of pattern transfer at resolutions below screen-printable limits. Compatibility testing with standard MEMS processes and materials was conducted to assess the potential of using standard physical masking techniques (table 1). To test etch performance, carbon test coupons were fabricated, as previously described. Additional test coupons with photoresist (AZ 4903, Mays Chemical, Indianapolis, IN) and Parylene C (Specialty Coating Systems, Indianapolis, IN) were also

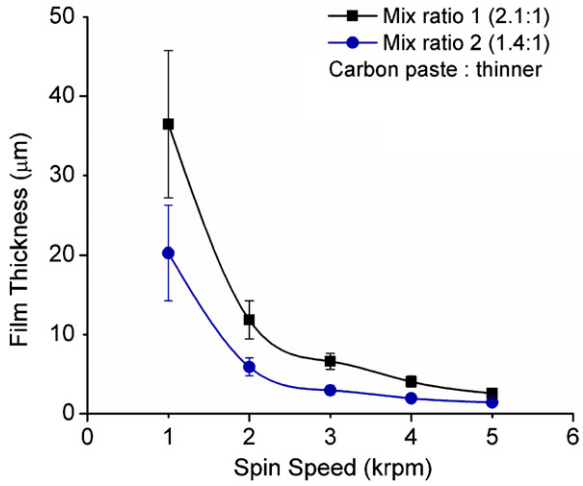

Figure 3. Film thickness as a function of spin speed measured on standard 75 × 50 mm laboratory glass slides. Carbon paste was thinned with dipropylene glycol monomethyl ether (mean ± SD, $n = 4$).

prepared for relative etch rate comparisons (table 2). A physical contact mask was utilized to shield portions of the coupon while exposing the remaining areas. Photoresist and Parylene C films exhibited greater etch rates when compared with the carbon film under nearly all conditions, with maximum thick-film etch rates observed at 200 W, 100 mtorr etching conditions (RIE 80, Oxford Plasma Technology, Oxfordshire, UK).

Due to the chemical incompatibility of the carbon thick films with the photoresist (table 1) and the relatively poor selectivity (table 2), chromium was selected as the etch mask material to micropattern an array of carbon microelectrodes serving as test features. A 2000 Å layer of chromium was deposited by e-beam evaporation (Temescal, Edwards, Livermore, CA) and patterned in a chrome etchant (CR-7, Cyantek, Fremont, CA). The carbon film was then etched in oxygen plasma (150 W, 100 mtorr) for approximately 15 min.

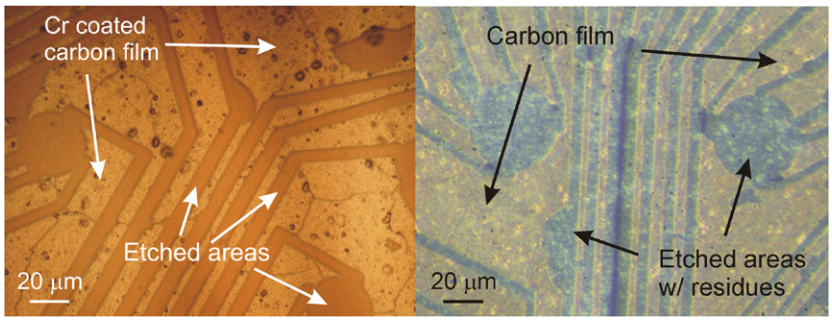

Figure 4. Alternate method of pattern transfer: RIE plasma etching with the chromium etch mask. (*a*) Optical micrograph of a patterned chromium mask over carbon film (carbon film roughness ±1 μm, 1–2 μm granule size). A uniform residue remains after etching. (*b*) After removal of the chromium mask, residue can clearly be seen in the optical micrograph. Non-volatile components of the carbon paste composition remain on the substrate.

Table 1. Carbon paste (Dupont 7082) MEMS process compatibility.

Process	Chemical	Result
Cleaning/rinsing	DI water	Compatible—no dissolution
Cleaning/rinsing	Isopropyl alcohol	Compatible—no dissolution
Photolithography	Photoresist	Not compatible—paste solvents attack photoresist
Photolithography	Photoresist developer	Compatible—no dissolution
Photoresist stripping and lift-off	Acetone	Not compatible—dissolves carbon film
Metal etching	Chrome etchant	Compatible—no dissolution

Table 2. RIE etch rate comparison (μm min^{-1}).

Power (W)	Pressure (mtorr)	Etch rate (μm min^{-1}) AZ 4903	Parylene C	Carbon
100	100	0.495	0.427	0.213
100	200	0.317	0.344	0.139
100	300	0.148	0.117	0.118
100	400	0.01	0.234	0.057
150	100	0.569	0.43	0.419
150	200	0.493	0.582	0.375
150	300	0.341	0.298	0.305
150	400	0.444	0.414	0.258
200	100	0.907	0.641	0.629
200	200	0.689	0.606	0.435
200	300	0.794	0.422	0.414
200	400	0.505	0.472	0.284

The result after the removal of the chrome mask is a clearly patterned film with residue evident in the regions exposed to the plasma (figure 4). The result indicates that although the carbon-particle filler appears to have been successfully etched away, there appears to be a non-organic or non-volatile component to the paste composition which is not easily removed in oxygen plasma. Due to incomplete material removal by RIE, this method of pattern transfer was not selected as the method of choice, although further work is necessary to fully characterize the exact nature of the post-etch residue.

2.4. Thick-film strain sensor fabrication

Biomedical grade silicone rubber (MDX4-4210, Silastic®, Dow Corning, Midland, MI) was prepared (AR-250 Hybrid Mixer, Thinky Corp., Tokyo, Japan) with a 10:1 base-to-curing-agent ratio. The prepolymer mix was poured onto a 75 × 50 mm standard laboratory glass slide (~500 μm thick), degassed in a vacuum and cured in a convection oven at ~80 °C for 30 min. The thick-film strain sensors were then screen printed onto the silicone sheet. Thin flexible 34AWG wire was then adhered to the carbon contact pads using a small drop of carbon paste at the contact pads. The films were cured in a convection oven at 120 °C for 30 min. The resultant thick films had a thickness of ~15 μm. A second layer of silicone (~500 μm) was then poured, degassed and cured to complete the encapsulation of the thick-film sensors (figure 5). A range of device designs of varying lengths and widths were fabricated, yielding unstrained resistances in the range of 3–70 kΩ (table 3).

Table 3. Strain sensor design parameters and measured unstrained resistances.

Design	Length (mm)	Width (μm)	Calculated resistance (kΩ)	Measured resistance (kΩ)
1	1	500	3	3–6
2	1.5	100	12	10–16
3	2.5	100	36	24–35
4	4.75	100	72	35–55
5	5.5	75	112	48–70

2.4.1. Multilayer thick-film sensor array fabrication. With the addition of an extra screen-printing step, the single-layer fabrication process can be extended to a multilayered process enabling low-resistance routing connections (figure 6). Due to the inherently high resistance of the carbon thick film

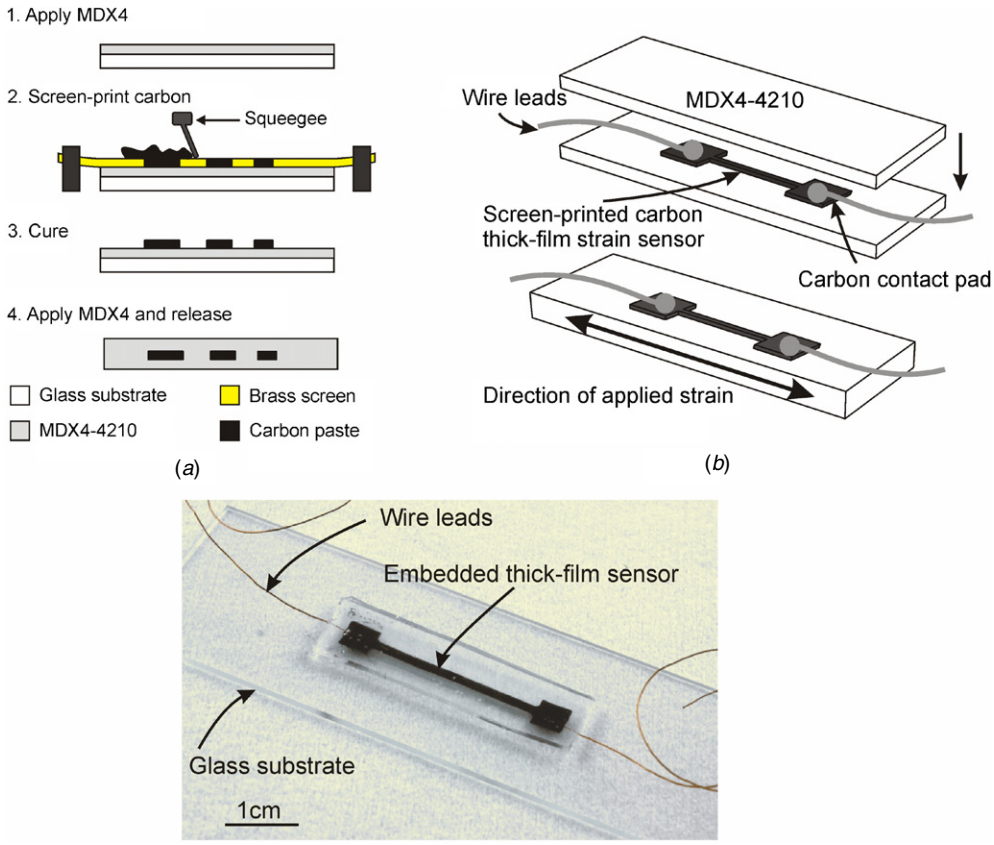

Figure 5. (*a*) Fabrication process for embedded carbon thick-film strain sensors within biomedical grade silicone. (*b*) Illustration of a single-layer carbon strain sensor embedded between PDMS layers. (*c*) Photograph of a carbon thick-film strain sensor with attached wires on a glass microscope slide (slide: 25 × 75 mm). Figure 5(b) reprinted from [17] with permission of the Transducer Research Foundation.

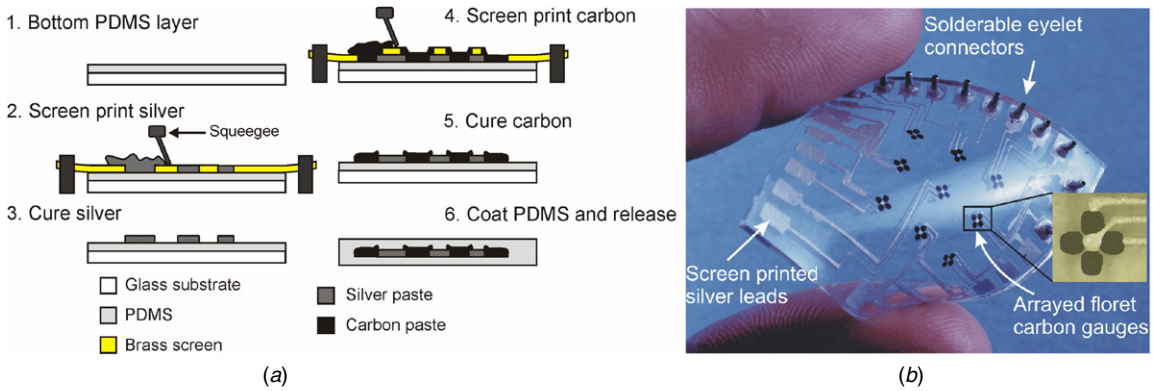

Figure 6. (*a*) Fabrication process for a flexible multilayered thick-film device with high-resistance sensors and low-resistance connective routing. (*b*) A fabricated 3 × 3 array of sensors in a floret configuration. Figure 6(*b*) reprinted from [17] with permission of the Transducer Research Foundation.

utilized here, it would be impractical to utilize the same material for both the sensing element and the connective wire routing within the substrate. This would yield an excessively high resistance contribution from the routing connection and obscure strain-responsive variations in the region of interest. Furthermore, strain response artifacts from the routing connections themselves could lead to confounding measurements. Therefore, the ability to pattern both high-resistance features with low-resistance routing connections within the same substrate enables additional sensor configurations. A proof-of-concept 3 × 3 array of 2-axis strain sensors in a floret configuration was fabricated using this method. High-conductivity silver paste was utilized as the routing material (Silver epoxy paste type 1, Transene Inc., Danvers, MA, USA). It was patterned onto the silicone substrate and then cured in an oven. The silver pattern was then aligned manually under a microscope to the carbon screen prior to printing of the carbon features. The carbon thick film was

deposited directly on top of the cured silver pattern followed by one more curing step to set the carbon. The silver was printed first because of the higher curing temperature required, thereby preventing excessive baking of the carbon material.

3. Experimental methods

3.1. Preparation of carbon films for sheet resistance measurements

Rectangular carbon films measuring 35 × 45 mm and with thicknesses ranging from 8.6 to 22.5 μm were screen printed onto standard 75 × 50 mm laboratory glass slides for sheet resistance measurements. The films were cured in a convection oven at 120 °C for 30 min. Sheet resistance is a useful measure of resistance for devices utilizing a single layer of resistive material with uniform thickness. Sensor resistance can easily be determined in the design stage if the sheet resistance is known. Furthermore, thick-film sheet resistance, in particular, is coupled to the GF, which is an important figure-of-merit for strain sensing technology [14]. Units of sheet resistance are expressed as Ω/□ or 'ohms-per-square'. The resistance scales linearly with the number of squares (of any side length) that can be drawn in the footprint of the resistive film.

A four-point probe measurement technique was utilized to assess the sheet resistance R_s given by

$$R_s = \frac{\pi}{\ln(2)}\left(\frac{V}{I}\right), \quad (1)$$

where $\pi/\ln(2) = 4.53$ for an infinite sheet. This expression is only valid for equal probe spacing between all four probes. For film thicknesses <40% of probe spacing, and if the edges of film are more than about four times the spacing distance from the measurement point, no correction factor is necessary [18–20]. Standard probe spacing is usually about 1 mm for most four-probe measurement systems, making it relatively easy to fabricate large area films by screen printing for accurate sheet resistance characterization. A four-point probe resistivity stand (302, Lucas Labs, Gilroy, CA) was used to measure sheet resistance. A sourcemeter (Keithley 2400, Keithley, Cleveland, OH) was used in 4-wire sense mode to simultaneously supply current and measure voltage.

3.2. Uniaxial loading apparatus

A dynamic mechanical testing system (ELF3100, Bose Corp., Eden Prairie, MN) was used to apply controlled strain to the microsensors while the resistance was simultaneously monitored with a precision multimeter (Keithley 2400, Keithley Instruments, Cleveland, OH).

The sensors were mounted to the test apparatus via specimen clamps with a known separation distance (figure 7). The clamp separation distance was computer controlled and was increased by discrete steps (minimum size 0.4 μm) thereby applying known levels of uniaxial strain. Sensor performance in low (<0.1%) and high (0.1–2%) strain regimes was evaluated. Various sensor designs were tested (table 3) under these two loading conditions. Low-strain loading allows for comparison of GF performance across several

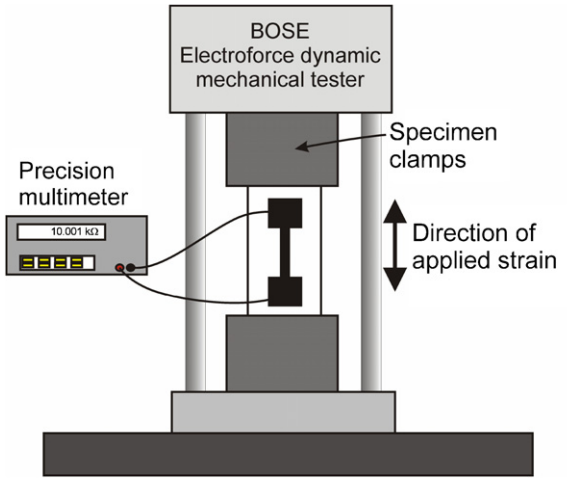

Figure 7. Schematic of the uniaxial strain measurement setup.

device designs while high-strain loading tests the ultimate yield strength and fracture limits of the thick-film material in addition to assessing linearity and performance for high-strain applications. Both of these loading conditions are important in determining the most appropriate sensor design for bladder wall strain measurement applications.

3.3. Temperature dependence characterization and soak testing

Temperature dependence characterization was conducted on three devices which were placed in an environmental chamber oven and connected to a precision multimeter (Keithley 2400, Keithley, Cleveland, OH) for resistance measurements. The chamber temperature was increased from ambient room temperature (23 °C) to a maximum of 80 °C by increments of 10 °C. The resistance of each device was recorded at each temperature point after allowing the system to reach thermal equilibrium.

Long-term soak testing was also conducted on three devices completely immersed in a 1× phosphate-buffered saline (PBS) solution. PBS provides an ionic environment similar to that found in the body. The solution and devices were maintained in a sealed container at core body temperature (37 °C) for the duration of the experiment. Resistance measurements were taken initially once every day with a maximum interval of three days towards the end of the 50 days of testing, at which point the experiment was concluded.

3.4. Bladder model

To replicate strain sensor monitoring of bladder fullness, a custom-engineered bladder model consisting of a latex sheet (500 μm thick) mounted in a laser-machined fixture (10 cm diameter opening) was constructed. Precise control of inflation/deflation of the bladder, and thus the applied strain, was achieved using a calibrated air pressure system. Sensors were mounted to the latex surface with a cyanoacrylate-based USP Class VI biomedical adhesive (MG 100, Adhesive System Inc, Frankfort, IL) (figure 8).

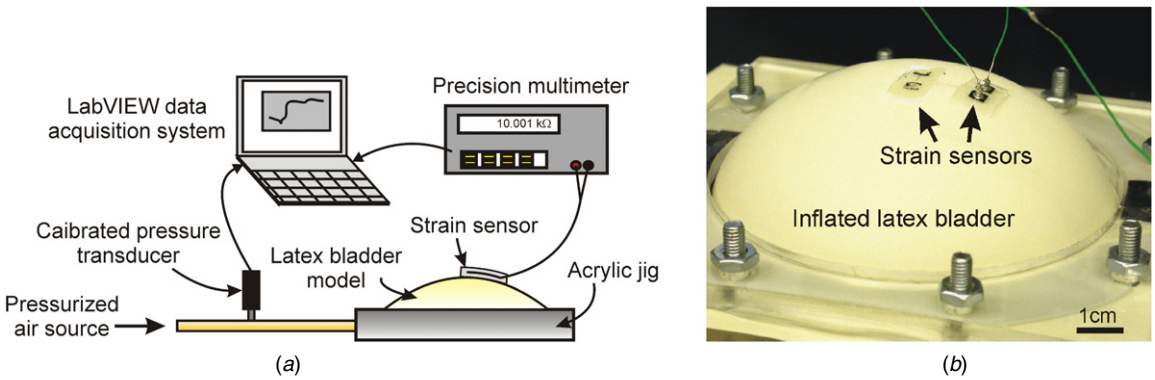

Figure 8. (*a*) Schematic of the bench-top bladder model setup. (*b*) Photograph of a custom-engineered latex bladder setup. Strain sensors attached to the latex wall responded to applied strain arising from controlled inflation of the model bladder. Figure 8(*b*) reprinted from [17] with permission of the Transducer Research Foundation.

Sensor resistance was monitored while internal bladder pressure was varied and recorded.

3.5. Directional discrimination capability of multilayered sensor arrays

The directional discrimination capability of dual-axis floret-configured multilayered strain sensors was evaluated. Several floret elements within the array were selected and monitored. The real time resistance response of a single floret sensor element was measured under single-axis loading during application of parallel and orthogonal strain to test the on-axis/off-axis resistance response. Strain was applied manually in lateral directions with approximately equal magnitude.

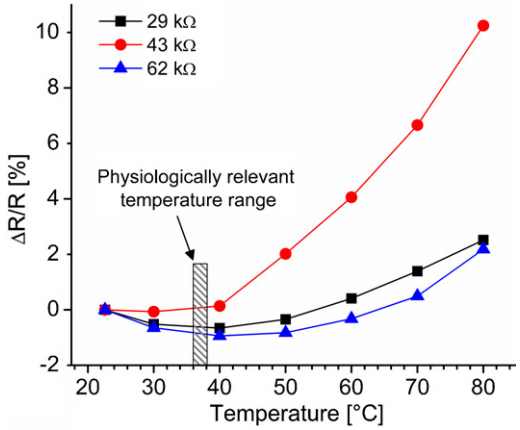

Figure 9. Resistance–temperature dependence.

4. Results and discussion

4.1. Sheet resistance measurements

Carbon films were fabricated for resistivity and sheet resistance characterization, as described previously. These measurements yielded an average resistivity of 1.50 ± 0.045 Ω cm (mean ± SD, $n = 4$), yielding an average sheet resistance of 1 kΩ $\square^{-1}$ for 15 μm thick films. When compared to sheet resistance values typically attained for metals, the values achievable with the carbon thick film were several orders of magnitude greater. The high resistance simplifies the layout of carbon sensing elements, which obviates the need for serpentine structures usually required by thin-film metal sensors to achieve appreciable resistances, thus minimizing overall sensor footprint. Based on these results, a straightforward 'strip' design was selected, providing direct resistance measurement capability, small footprint and strain measurement along one axis.

Generally, there exists a relationship between the sheet resistance and the GF for thick films. For films with sheet resistances less than about 1 kΩ $\square^{-1}$, GFs of about 2 are typically observed, while for films with sheet resistances greater than about 100 kΩ $\square^{-1}$, GFs up to 12 are typically observed [14, 15, 21–24]. Thus increasing the sheet resistance generally leads to increased GF and therefore sensitivity. Increasing sheet resistance could potentially be achieved by using thinner films or by alternative paste recipes with lower carbon content. The drawback of using a thinner film is that the film becomes more fragile and film fracture may occur at lower strain levels. Additionally, due to the fairly large grain size (1–2 μm) found in the paste composition, a homogenous film requires thicknesses of ∼10 μm to avoid cracking during the curing process. A modest increase in sheet resistance would therefore be possible at the cost of film durability. The measured sheet resistance is, however, still sufficient for the intended application. Characterization of the GF for the thick-film 'strip' sensors fabricated here is discussed in later sections.

4.2. Resistance–temperature dependence

The measured temperature dependence was parabolic across all devices measured (figure 9). This parabolic resistance–temperature characteristic is a well-documented phenomenon for thick-film materials. Several theories have been put forward to explain this behavior, including electron percolation theory [25] (commonly employed to explain the charge-transport mechanism in semiconductors [26, 27]).

However, the most widely accepted theory proposed by Sion *et al* [28] argues that a combination of thermal coefficient of expansion (TCE) and thick-film thermal coefficient of resistance (TCR) produces the parabolic dependence. It was

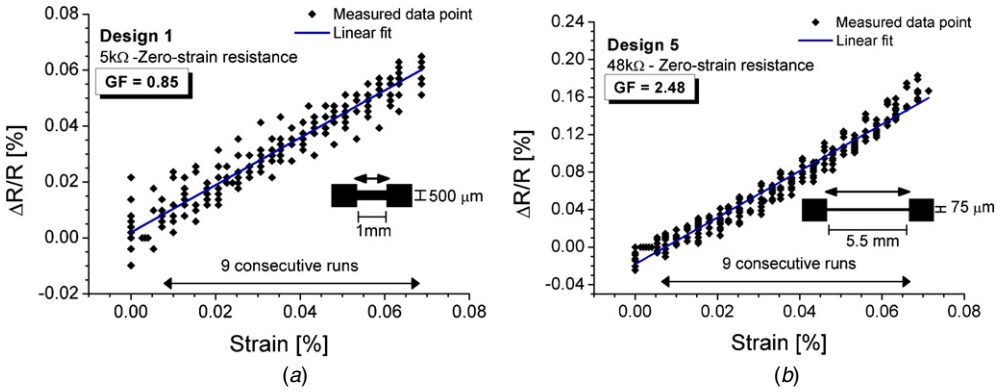

Figure 10. Data from nine consecutive strain cycles were plotted for two devices: designs 1 and 5 (as per table 3). (*a*) Strain sensitivity for a 5 kΩ device. (*b*) Strain sensitivity for a 48 kΩ device. The maximum GF achieved was ∼2.5 with design 5.

shown conclusively that the combination of the exponential temperature characteristics of resistivity for thick-film resistors (TFRs) and the effects of thermal strain arising from TCE mismatch between the TFR and substrate produced the parabolic characteristic.

For *in vivo* applications, sensor performance over a wide temperature range is not as important as understanding the sensitivity to temperature variations near body temperature. The *in vivo* environment is considered to be highly temperature stable, with thermal fluctuations not exceeding ±1 °C from the average core body temperature (37 °C). The result for three carbon sensors tested indicates that the inflection point of parabolic curve lies close to 37 °C. This is beneficial because it implies that small temperature variations around core body temperature will have a minimal effect on resistance measurements. Maximum error introduced by temperature fluctuations in an *in vivo* setting is estimated to be within 0.1% (figure 9). This makes it possible to attain reliable strain measurement data without the need for additional temperature compensation circuitry, further simplifying sensor implementation.

4.3. Soak testing

To further verify the suitability for long-term implantation and performance, three sensors were passively and continuously soaked in PBS at 37 °C to simulate *in vivo* conditions. No degradation in sensor resistance was observed after 50 days of passive soaking, at which point the experiment was concluded. Furthermore, there was no visible degradation of the silicone substrate nor migration of any carbon materials through the substrate. The positive results validate the fabrication process and verify the encapsulation capability of MDX-4 for thick-film sensors *in vivo*.

4.4. Uniaxial strain measurement

Sensor performance in low (<0.1%) and high (0.1–2%) strain regimes were evaluated. Low-strain testing was conducted on three representative sample devices: designs 1, 3 (data not shown) and 5 as per table 3. The data in figure 10 were generated by nine consecutive loading and unloading cycles per device. Generally, all sensor designs exhibited a positive linear response with strain. Design 1 (adj. $R^2 = 0.980$) exhibited the lowest sensitivity (GF ∼0.85), while design 5 (adj. $R^2 = 0.974$) exhibited the highest sensitivity (GF ∼2.5). High-resistance devices (design 5) provided a more uniform and repeatable response that was, however, somewhat less linear over this loading range. Although good linearity was observed with all designs, hysteresis during loading/unloading cycles contributed to overall strain measurement errors and limited measurement accuracy for low-resistance designs (figure 10(*a*)). A strain measurement accuracy of ±14.3% of full scale (0.07% strain) was achieved with design 1 providing very limited performance for low-strain applications. An absolute strain measurement resolution of ±0.005% was achieved with high resistance sensors (design 5) and this includes all measurement and hysteresis errors over the nine loading cycles. Over the range of operation (0–0.07% strain), this yields a measurement accuracy of ±7.14% of full-scale, suggesting that under low-strain conditions, high-resistance sensors provide an optimum combination of sensitivity, accuracy and repeatability. Long-term loading and fatigue testing are still required to assess strain measurement performance over prolonged periods of cyclic stress.

High-strain loading was conducted on five samples (designs 1–5). Each sensor was tested once until fracture was observed or until approximately 2% applied strain was achieved. For sensors in which fracture occurred, no further data were collected. For sensors that did not fracture, a single loading/unloading cycle was recorded (figure 11). Under high-strain loading conditions, high zero-strain resistance devices (>20 kΩ, designs 3–5) exhibited a nonlinear response followed by fracture of the carbon pattern (indicated by an open circuit reading). The points of fracture were clearly visible under an optical microscope, but the silicone rubber substrate remained intact. Fracture generally occurred in the range of 1–1.5% strain. As strain was reduced during the unloading cycle, the separated carbon sensor segments were brought back into contact as indicated by a finite resistance reading. These results further suggest that high zero-strain resistance designs are most suitable for low-strain applications.

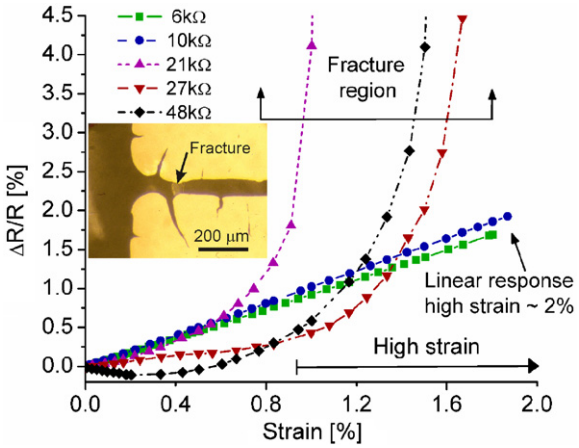

Figure 11. High-strain loading performance for five different device designs. Reprinted from [17] with permission of the Transducer Research Foundation.

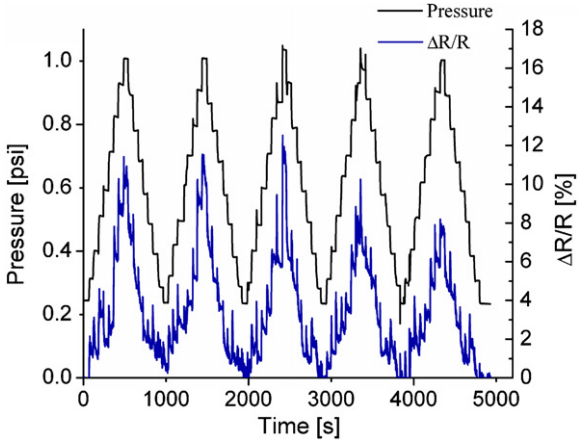

Figure 12. Representative data demonstrating real-time pressure tracking by a strain sensor (5 kΩ) attached to the latex bladder wall. Reprinted from [17] with permission of the Transducer Research Foundation.

Low zero-strain resistance devices (<10 kΩ) exhibited a very linear response up to 2% strain with no breakage or cracking of the carbon film observed. Over this range, no noticeable hysteresis was observed but multiple loading/unloading cycles were not performed. The measurement performance of low-resistance devices (designs 1 and 2) in this range of applied strain is significantly better than under low-strain loading conditions. Measurement errors over this range were estimated to be within ±0.75% of full scale. In the context of bladder strain applications where large strain variations are expected, the performance of low-resistance devices appears to be more suitable. We therefore found low zero-strain resistance designs both more robust and linear over a wider range of strain, and these would be preferred for bladder strain measurement applications.

4.5. Bladder performance

Pressures up to 1 psi (6.89 kPa) were applied corresponding to maximum strains of 30–40% on the latex bladder surface. The pressure and thus strain was successfully tracked by monitoring the resistance of a sensor (5 kΩ—design 1) mounted to the latex surface (figure 12). The bladder underwent multiple inflation/deflation cycles over a period of 83 min under continuous monitoring. Although the measured strains are greater than previously tested limits of the sensors, there are at least two factors that contribute to the observed behavior. The first is that the relatively stiff mounting adhesive between the sensor and bladder dampens and limits the strain transmitted to the sensor. This highlights the need for an appropriate fixation method. The second factor is that the bladder model applies a combination of tangential and radial strains rather than simple uniaxial strain. Due to sensor placement near the center of the bladder (where tangential and radial strains are equal) and the presence of the adhesive, the total strain is distributed and dampened, allowing the sensors to capture bladder inflation dynamics without fracture failure [29].

Relaxation in the latex sheet after repeated inflation/deflation cycles was a significant factor in consistent measurements. A 'break-in' period was required for both the latex sheet and the attached sensor to achieve steady measurements. However, after repeated cycling, sheet relaxation resulted in a decreased sensor response for the same applied bladder pressure during later cycles. Steady-state strain measurements were also conducted at intermediate pressures (0.4, 0.6, 0.8 psi) and confirmed that the sensors were capable of tracking sustained levels of steady-state strains over a period of 10 min.

4.6. Multilayer sensor array dual-axis capability

A clear difference in the response between the on-axis (parallel) and off-axis (orthogonal) strain was consistently observed across several devices (figure 13). Elongation of a sensor element along a particular axis may also provide increased sensitivity along that axis while simultaneously reducing directional cross-talk. The floret configuration is very compact (1.5 mm^2) and is well suited to applications requiring an array of multi-axis sensors. Directional discrimination within a monolithic film enables potentially interesting applications to complex systems with anisotropic strain profiles. For example, the electrically evoked contractile response of muscle tissues could be monitored by a multi-axis strain sensor array affixed to the tissue surface. Multi-axis strain information from such a system could provide feedback regarding optimum electrical stimulation parameters, such as timing, frequency and amplitude, and help in the design and placement of stimulation electrodes for advanced prosthetic systems.

4.7. Suitability for in vivo applications

Commercially available strain sensors are commonly packaged in a flexible plastic substrate, such as polyimide, while solid-state semiconductive sensors utilize silicon as the substrate material. These sensors typically employ piezoresistive materials, such as metals (i.e. gold, platinum and other alloys) and semiconductors. Both have a long,

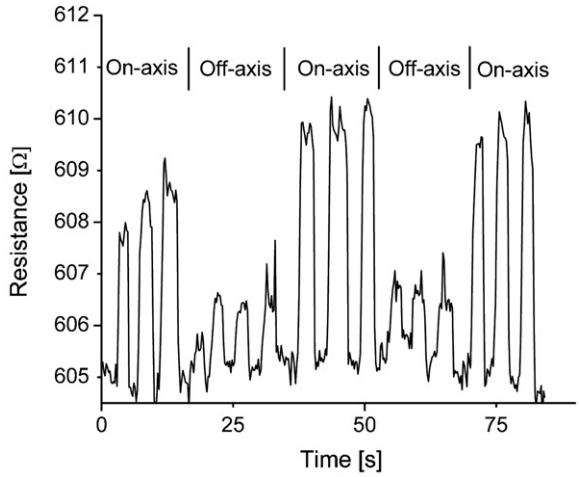

Figure 13. Resistance measurements of single floret sensor element. Strain was applied manually in orthogonal lateral directions to test the on-axis/off-axis resistance response. Some cross-talk was observed, but a larger on-axis response is clearly obtained. The figure is representative of a typically observed response. Reprinted from [17] with permission of the Transducer Research Foundation.

extensive history in strain sensor design [30, 31]. However, these traditional approaches are most suitable for low-strain conditions (<0.1%). Measurement of bone strain has been demonstrated *in vivo* [32] with traditional thin-film sensors. However, the low-strain, high-stiffness conditions specific to bone are not applicable to soft tissues found throughout the body. Furthermore, fabrication of sensors with these materials generally requires clean room facilities to deposit and pattern thin films. Following fabrication, extensive packaging and assembly steps are typically required for *in vivo* use, adding further complexity and cost. Although commercial sensors are relatively inexpensive (due to economies of scale) and simple to use, there exist several factors limiting their application *in vivo*. A major drawback of solid-state silicon sensors is their inability to provide cost-effective solutions to niche problems with low to medium (1–10 thousand per year) production volume requirements [9]. Additionally, there exists a large mechanical mismatch between soft tissues and common substrates, such as polyimide and silicon. Such substrate materials can be up to five orders of magnitude stiffer than soft tissue (table 4). This mismatch makes it extremely difficult to employ such sensors *in vivo*. Silicone rubbers possess mechanical properties that more closely match those of soft tissue, like the bladder. Furthermore, the final mechanical properties of the rubber can easily be adjusted by changing the ratio of elastomer to curing agent in the prepolymer mixture.

For these reasons, thick-film-based strain sensors offer several advantages over traditional approaches for *in vivo* applications. Thick films are straightforward to implement, compatible with established microfabrication techniques and inexpensive to process when compared with traditional metal thin-film strain sensors. Furthermore, thick-film patterns are readily microfabricated on flexible polymer substrates that provide superior mechanical matching to soft tissues over traditional rigid substrates [38, 39, 41]. These advantages, coupled with the superior encapsulation

Table 4. Young's modulus of common strain sensor substrate materials and relative processing costs for small-medium production volume. For comparison, the modulus of soft tissue is included.

Material	Young's modulus (MPa)	Processing cost
Soft tissue	∼ 0.1 [33–37]	n/a
Silicone rubber	0.2–0.5 [38, 39]	Low
Silicone	130 000 [31, 40, 41]	High
Polyimide	∼ 7500 [41]	Low-medium
Parylene-C	∼ 4000 [42, 43]	Low-medium

performance of biomedical grade silicone rubber and the relatively flat temperature dependence (at physiologically relevant conditions) of the thick films utilized here, make this combination of materials well suited to implantable applications.

The feasibility of measuring bladder strain with thick-film sensors has been demonstrated here, but consideration of the final attachment mechanism and location is still required for *in vivo* use. Various attachment parameters, including suture material and sensor location, were investigated previously in goats [4]. It was found that devices sutured superficially on the bladder wall (peritoneum) detached within 12 months. Furthermore, devices sutured within the wall (between the bladder muscle and internal bladder epithelium) failed due to erosion through the epithelium into the bladder lumen. The most promising attachment location was found to be between the bladder muscle and peritoneum with non-absorbable polypropylene sutures. A simple modification to the current sensor design can include reinforced suture holes through which the device can be easily attached to this location *in vivo*.

Our present study has focused on characterizing single 'strip' devices of varying lengths and widths, 1–5.5 mm and 75–500 μm, respectively, with a total device thickness of approximately 1–2 mm. Further refinement of sensor design would allow for more precise targeting of the physiologically relevant strains encountered during bladder filling and voiding. The bladder possesses a remarkable wall structure that can accommodate both large distensions (up to 11 times its resting volume [35]) during normal urine filling as well as rapid release back to a relaxed resting state. Bladder wall strain ratios up to 70% are possible [5]. Therefore, designing a sensor capable of operation within an acceptable range of strain, for example in achieving >80% voiding efficiency [44, 45], is required. By controlling the device thickness, the strain response to applied stress can be modified. Thicker devices will experience less deformation under the same loads when compared with thinner devices. In this manner, an optimum combination of device robustness and response can be achieved. Similarly, the elasticity of the silicone substrate material can be tailored by adjusting the prepolymer to curing agent ratio. Additional sensor layouts can also be considered that extend the strain measurement capability of this technology. For instance, a cross-hatched or interleaved sensor pattern can be created. Additionally, the silicone substrate itself can also be patterned in a similar manner by cutting or coring out unused and unpatterned regions. The resulting strain-sensitive 'mesh' will

be much more responsive to imposed stresses than a solid slab of the same footprint. This technique can improve sensor robustness and strain measurement range when piezoresistive materials of low yield strength, such as thin-film metals, are utilized [46]. The ability to easily modify sensor design parameters allows the fabrication of a range of device and material properties that can be engineered to closely match those of the bladder and to operate within its physiological range.

5. Conclusion

Simple, robust, low-cost carbon thick-film-based sensors were designed, fabricated, tested and shown to be effective in measuring bladder fullness and strain on a bench-top model. A straightforward cost-effective fabrication process was utilized without the need for large, expensive equipment or facilities. The use of USP class VI and ISO 10993-1 approved medical-grade encapsulation and adhesive materials enables the use of these sensors for various implantable applications. The strain sensitivity and performance of these sensors were investigated using uniaxial strain measurements and a bench-top bladder model, with positive results demonstrating the ability to measure large strains at physiologically relevant strain levels. Temperature dependence and soak testing performance were characterized and validated for the *in vivo* environment. The fabrication process can also be extended to include multilayer devices for arrayed applications. Future work can include wireless telemetry for external measurements as well as integration with preclinical neuroprosthetic systems currently under development in animal models. This work provides a starting point for the fabrication of various other thick-film-based technologies intended for use with implantable medical devices where closed-loop operation and sensory feedback information are required.

Acknowledgments

This work was supported in part by the Engineering Research Centers Program of the NSF under Award Number EEC-0310723, an NSF CAREER Award (ECS-0547544) and the Bill and Melinda Gates Foundation (CG). We would like to thank Ms Alice Cho for assistance in performing uniaxial strain studies and Mr Jason Geathers and Mr Lawrence Yu for assistance in fabrication. We would also like to thank Professor James Weiland for access to the Bose ELF3100 mechanical testing system.

References

[1] Spinal Cord Injury Information Network *Spinal Cord Injury Facts & Figures at a Glance 2009* [cited 2009 October 12] Available at http://www.spinalcord.uab.edu/show.asp?durki = 119513&site = 4716&return = 19775

[2] Benevento B T and Sipski M L 2002 Neurogenic bladder, neurogenic bowel, and sexual dysfunction in people with spinal cord injury *Phys. Ther.* **82** 601–12

[3] Korkmaz I and Rogg B 2007 A simple fluid-mechanical model for the prediction of the stress-strain relation of the male urinary bladder *J. Biomech.* **40** 663–8

[4] Koldewijn E L, Van Kerrebroeck P E, Schaafsma E, Wijkstra H, Debruyne F M and Brindley G S 1994 Bladder pressure sensors in an animal model *J. Urol.* **151** 1379–84

[5] Rajagopalan S, Sawan M, Ghafar-Zadeh E, Savadogo O and Chodavarapu V P 2008 A polypyrrole-based strain sensor dedicated to measure bladder volume in patients with urinary dysfunction *Sensors* **8** 5081–95

[6] Coosemans J and Puers R 2005 An autonomous bladder pressure monitoring system *Sensors and Actuators* A **123–24** 155–61

[7] Creasey G H, Grill J H, Korsten M, U H S, Betz R, Anderson R and Walter J 2001 An implantable neuroprosthesis for restoring bladder and bowel control to patients with spinal cord injuries: a multicenter trial *Arch. Phys. Med. Rehabil.* **82** 1512–9

[8] Gaunt R A and Prochazka A 2006 Control of urinary bladder function with devices: successes and failures *Autonomic Prog. Brain. Res.* **152** 163–94

[9] White N M and Turner J D 1997 Thick-film sensors: past, present and future *Meas. Sci. Technol.* **8** 1–20

[10] George P M, Muthaswamy J, Currie J, Shakor N V and Paranjape M 2001 Fabrication of screen-printed carbon electrode array for sensing neuronal messengers *Biomed. Microdevices* **3**(4) 307–13

[11] Engel J M, Chen J, Chen N, Pandya S and Liu C 2005 Development and characterization of an artificial hair cell based on polyurethane elastomer and force sensitive resistors *Proc. IEEE Sensors* pp 1014–7

[12] Berg C A, Cumpston H and Rinsky A 1972 Piezoresistance of graphite fibers *Text. Res. J.* **42** 486

[13] Frazier B A and Allen M G 1993 Piezoresistive graphite/polyimide thin films for micromachining applications *J. Appl. Phys.* **73** 4428–33

[14] Brignell J E, White N M and Cranny A W J 1988 Sensor applications of thick-film technology *IEE Proc.* I **135** 77–84

[15] Shah J S 1980 Strain sensitivity in thick-film resistors *IEEE Trans. Compon., Hybrids, Manuf. Technol.* **3** 554–64

[16] Prudenziati M and Morten B 1986 Piezoresistive properties of thick-film resistors: an overview *Microelectronics International* **3** 20–37

[17] Gutierrez C A, Cho A, Geathers J, Yu L, Abram T and Meng E 2009 An implantable low-cost multilayered screen-printed carbon thick-film strain sensor *Proc. Microtechnologies in Medicine and Biology (Quebec City, Canada)* pp 128–9

[18] Valdes L B 1954 Resistivity measurements on germanium for transistors *Proc. IRE* vol. 42 pp 420–7

[19] Smits F M 1957 Measurement of sheet resistivities with the four-point probe *Bell Syst. Tech. J.* **37** 711–8

[20] Bridge Technology *Four Point Probe Theory* (cited 23 October 2009) Available at http://www.four-point-probes.com/probelife.html

[21] Arshak K I, Ansar F and Collins D 1994 Analysis of thick-film strain resistors on stainless steel and ceramic substrates *Int. J. Electron.* **76** 365–76

[22] Canali C, Malavisi D, Morten B and Prudenziati M 1980 Piezoresistive effects in thick-film resistors *J. Appl. Phys* **51** 3282–6

[23] White N and Cranny A 1987 Design and fabrication of thick-film sensors *Hybrid Circuits* **12**

[24] Prudenziati M, Morten B and Taroni A 1983 Thick-film technology and sensors *Sensors Actuators* **4** 237–45

[25] Forlani F and Prudenziati M 1976 Electrical conduction by percolation in thick film resistors *Electrocompon. Sci. Technol.* **3** 77–83

[26] Miller A and Abrahams E 1960 Impurity conduction at low temperatures *Phys. Rev.* B **120** 745–55

[27] Ambegaoker V, Halperin B I and Langer J S 1971 Hopping conductivity in disordered systems *Phys. Rev.* B **4** 2612–20

[28] Sion R P, Atkinson J K and Turner J D 1994 A novel model for the temperature characteristic of a thick-film piezoresistive sensor *Sensors Actuators* **41–42** 460–4
[29] Schomburg W K, Rummler Z, Shao P, Wulff K and Xie L 2004 The design of metal strain gauges on diaphrams *J. Micromech. Microeng.* **14** 1101–8
[30] Yang G Y, Johnson G, Tang C W and Keyak J H 2007 Parylene-based strain sensors for bone *IEEE Sensors* **7** 1693–7
[31] Higson G R 1964 Recent advances in strain gauges *J. Sci. Instrum.* **41** 401–5
[32] Szivek J A and Magee F P 1989 A long-term *in vivo* bone strain measurement device *J. Invest. Surg.* **2** 195–206
[33] Agache P G, Monneur C, Leveque J L and De Rigal J 1980 Mechanical properties and Young's modulus of human skin *in vivo Arch. Dermatol. Res.* **269** 221–32
[34] Escoffier C, de Rigal J, Rochefort A, Vasselet R, Leveque J L and Agache P G 1989 Age-related mechanical properties of human skin: an *in vivo* study *J. Invest. Dermatol.* **93** 353–7
[35] Gloeckner C D 2003 Tissue biomechanics of the urinary bladder wall *Bioengineering* (Pittsburgh: University of Pittsburgh Press)
[36] Miller K, Chinzei K, Orssengo G and Bednarz P 2000 Mechanical properties of brain tissue *in-vivo*: experiment and computer simulation *J. Biomech.* **33** 1369–76
[37] Hammer M E, Peters W H and Wu W 1987 Basic mechanical properties of retina in simple elongation *J. Biomech. Eng.* **109** 65–7
[38] Armani D, Liu C and Aluru N 1999 Re-configurable fluid circuits by PDMS elastomer micromachining *Proc. IEEE Int. Conf. on MEMS* pp 222–7
[39] Lotters J C, Olthuis W, Veltink P H and Bergveld P 1997 The mechanical properties of polydimethylsiloxane for sensor applications *J. Micromech. Microeng.* **7** 145–7
[40] Butta E, Petris S D and Pasquini M 1969 Youngs modulus and secondary mechanical dispersion of polypyromellitimide *J. Appl. Polym. Sci.* **13** 1073–81
[41] Harper C A 1996 *Handbook of Plastics, Elastomers, and Composites* (Lutherville, Maryland: McGraw-Hill)
[42] Cookson Specialty Coating Systems http://www.Scscoatings.Com/parylene knowledge/ specifications
[43] Wolgemuth L 2000 Assessing the performance and suitability of parylene coating *Med. Device Diagn. Ind.* **22** 42–9
[44] Pikov V, Bullara L and McCreery D B 2007 Intraspinal stimulation for bladder voiding in cats before and after chronic spinal cord injury *J. Neural Eng.* **4** 356–68
[45] Tai C, Booth A M, de Groat W C and Roppolo J R 2004 Bladder and urethral sphincter responses evoked by microstimulation of s2 sacral spinal cord in spinal cord intact and chronic spinal cord injured cats *Exp. Neurol.* **190** 171–83
[46] Meacham K W, Giuly R J and Guo L 2008 A lithographically-patterned, elastic multi-electrode array for surface stimulation of the spinal cord *Biomed. Microdevices* **10** 259–69